PNAS RESEARCH ARTICLE | NEUROSCIENCE

# Mapping developmental regionalization and patterns of cortical surface area from 29 post-menstrual weeks to 2 years of age

Ying Huang[a,b], Zhengwang Wu[b], Fan Wang[b], Dan Hu[b], Tengfei Li[b], Lei Guo[a], Li Wang[b], Weili Lin[b], and Gang Li[b,1]

Edited by Marcus Raichle, Washington University in St. Louis, St. Louis, MO; received December 3, 2021; accepted June 27, 2022

**Surface area of the human cerebral cortex expands extremely dynamically and regionally heterogeneously from the third trimester of pregnancy to 2 y of age, reflecting the spatial heterogeneity of the underlying microstructural and functional development of the cerebral cortex. However, little is known about the developmental patterns and regionalization of cortical surface area during this critical stage, due to the lack of high-quality imaging data and accurate computational tools for pediatric brain MRI data. To fill this critical knowledge gap, by leveraging 1,037 high-quality MRI scans with the age between 29 post-menstrual weeks and 24 mo from 735 pediatric subjects in two complementary datasets, i.e., the Baby Connectome Project (BCP) and the developing Human Connectome Project (dHCP), and state-of-the-art dedicated image-processing tools, we unprecedentedly parcellate the cerebral cortex into a set of distinct subdivisions purely according to the developmental patterns of the cortical surface. Our discovered developmentally distinct subdivisions correspond well to structurally and functionally meaningful regions and reveal spatially contiguous, hierarchical, and bilaterally symmetric patterns of early cortical surface expansion. We also show that high-order association subdivisions, where cortical folds emerge later during prenatal stages, undergo more dramatic cortical surface expansion during infancy, compared with the central regions, especially the sensorimotor and insula cortices, thus forming a distinct central-pole division in early cortical surface expansion. These results provide an important reference for exploring and understanding dynamic early brain development in health and disease.**

cortical surface area | early brain development | developmental regionalization

## Significance

Perinatal and early postnatal development of cortical surface area is essential for establishing cognitive abilities and behaviors that could impact an entire lifetime. Investigating the developmental regionalization and patterns of cortical surface area during this critical age can advance our understanding of the underlying mechanisms of normal brain development. Thus, we unprecedently leveraged >1,000 infant MRI scans from two large-scale infant neuroimaging datasets, which seamlessly cover both perinatal and postnatal periods, and discovered the developmentally distinct cortical parcels that correspond well to structurally or functionally meaningful regions. Moreover, an obvious central-pole separation with high-order association cortices undergoing more dramatic expansion than central regions was also unveiled. The results greatly compensate for the deficiencies of the previous knowledge of early cortical development.

The human brain development is a complex and long-lasting process that starts from conception and lasts until the end of adolescence (1–3). Particularly, during the third trimester of pregnancy and early postnatal stages, the human brain undergoes exceptionally intensive development of cortical volume and cortical folding (4–7), which are associated with increases in both surface area and cortical thickness, each having distinct developmental patterns (8–10). In fact, in comparison to the development of cortical thickness, cortical surface area expands much more dynamically and largely drives the growth of the cerebral cortex during the perinatal and early postnatal stages (9, 11). The early dynamic development of cortical surface area is critical for establishing cognitive abilities and behaviors that could last an entire lifetime (12, 13).

For analysis of early brain development, increasing studies have been performed to delineate the cortical parcellations of neonates and infants in recent years (14–28). For example, based on anatomical information, several neonatal and infant cortical parcellation maps have been created either on the volumetric atlases [e.g., JHU-neonate-SS atlas (26), Melbourne neonatal atlas (27), and UNC Infant 0-1-2 Atlases (23)] or cortical surface atlases [e.g., UNC 4D cortical surface atlases (18, 19, 21), dHCP surface atlas (20), and surface-based Melbourne atlases (28)]. In addition, based on functional connectivity patterns, infant-specific functional parcellations are also derived to define functionally homogeneous regions (22). Moreover, integrated structural and functional atlases of infant brains have been developed for better understanding coherent patterns of early brain anatomical and functional development (29). However, the currently available cortical parcellations in neonates and infants typically don't take advantage of the rich information in the dynamic development of the cerebral cortex during infancy, which can help better define the developmentally distinctive cortical regions and understand early brain developmental mechanisms. To address this issue, a prior investigation has unveiled infantile developmental regionalization of cortical thickness (30), i.e., a spatial layout of developmentally distinct regions during infancy, each of which is composed of a set of codeveloping cortical vertices, differing remarkably from the conventional cortical parcellations and reflecting the underlying cellular nonuniformities and their heterogeneous development. Compared with cortical thickness, cortical surface area has its

Author contributions: Y.H. and G.L. designed research; Y.H. and G.L. performed research; Y.H., Z.W., F.W., T.L., L.W., and G.L. analyzed data; and Y.H., Z.W., F.W., D.H., L.G., L.W., W.L., and G.L. wrote the paper.

The authors declare no competing interest.

This article is a PNAS Direct Submission.



[1]To whom correspondence may be addressed. Email: gang_li@med.unc.edu.

This article contains supporting information online at http://www.pnas.org/lookup/suppl/doi:10.1073/pnas.2121748119/-/DCSupplemental.

Published August 8, 2022.

distinct genetic and cellular mechanisms and growth patterns (9, 31, 32); it is thus natural to speculate that cortical surface area will form its own distinct developmental regionalization. Moreover, the abnormal early development of cortical surface area is closely linked to neurodevelopmental and neuropsychiatric disorders, e.g., autism spectrum disorder and schizophrenia (33–38). Therefore, investigating the developmental regionalization of cortical surface area during early brain development may provide important insights into normal brain developmental mechanisms and patterns and their deviations in neurodevelopmental disorders, possibly guiding us to find the relevant biomarkers and formulate targeted interventions.

However, the developmental regionalization of cortical surface area during early brain development remains largely unexplored, due to the huge difficulties in the acquisition of large-scale, high-quality pediatric neuroimaging data and the lack of tailored computational techniques capable of processing pediatric brain imaging, typically with extremely low contrast and dynamic appearances. Although few pioneering studies have suggested region-specific surface area expansion during the first and second years, they are intrinsically limited by very sparse imaging time points (e.g., at 1 mo, 1 y, and 2 y of age), lack of data before term birth, small cohorts, and low imaging resolutions (9, 39). To fill this critical gap, in this paper, by combining two highly recognized and complementary large-scale pediatric neuroimaging datasets with a total of 1,037 high-resolution MRI scans from 29 post-menstrual weeks to 2 y of age, i.e., the developing Human Connectome Project (dHCP) (40) and the UNC/UMN Baby Connectome Project (BCP) (41), we precisely reveal the developmental regionalization and patterns of cortical surface area during perinatal and early postnatal stages. To this end, we employ a data-driven algorithm, namely nonnegative matrix factorization (NMF), to parcellate the cortex into different regions according to the developmental patterns of the surface area, without making assumptions of any linear or parametric relationships of growth patterns. For each discovered region, which is composed of a set of vertices sharing a similar developmental pattern, we further model the region-specific explicit developmental trajectory and delineate the regions that develop faster and lower than the whole cerebral cortex.

## Results

In this study, we first arranged the surface area map of each scan from BCP and dHCP datasets into a column to form a large nonnegative data matrix. Next, the NMF method was performed to group all cortical vertices into $k$ regions, and the appropriate region number $k$ was determined based on the criteria of silhouette coefficients and reconstruction errors. As our research focused on the relatively large-scale and primary structures in developmental regionalization as in (32, 42), we set the maximum $k$ as 20. And finally, we applied the generalized additive mixed models (GAMM) (43) to model the developmental pattern of surface area in each distinct region.

**Developmental Regionalization of Surface Area.** The discovered developmental regionalization maps (Fig. 1) exhibit bilaterally largely symmetric patterns across most of region numbers, despite that NMF was performed on both hemispheres simultaneously, without imposing any constraint for hemispheric symmetry. Moreover, as the region number increases, many new emerging regions tend to abide the boundaries of preceding regions, thus generating hierarchically meaningful developmental regionalization maps of the surface area. Specifically, when setting the region number as 2, we identified a distinct central-pole partition, which separates the high-order association (lateral prefrontal, temporal, and inferior parietal) and occipital cortices from sensorimotor, auditory, insular, and medial cortices. When increasing the region number to 3, the occipital cortex emerges as a new distinct region. Two representative boundaries indicated by green and orange arrows are continuously well preserved from 2 regions to 17 regions. Besides, the boundary between the superior temporal cortex and the middle temporal cortex (as indicated by black arrows) appeared when the region number is 5 and is well preserved till 17 regions. All these together suggest the meaningfulness of our discovered regionalization.

We utilized both silhouette coefficients and reconstruction errors to determine the appropriate region number. The local maximums of silhouette coefficients are reached when $k$ equals to 7 and 16 (Fig. 2*A*). Nevertheless, when $k$ equals to 7, the reconstruction error (Fig. 2*B*) is relatively higher; we thus adopted $k = 16$ regions as the appropriate developmental regionalization results of cortical surface area. However, the region colored in blue is composed of three spatially separated parts when the region number is 16 (Fig. 1). Therefore, we further divided this heterogenous region into three smaller, spatially continuous regions and thus obtained the final developmental regionalization map with 18 regions (Fig. 3*A*). It is worth to mention that all these 18 regions are bilaterally symmetric and largely correspond to structurally and functionally meaningful regions according to existing neuroscience knowledge (32,54). In accordance with the numbers and colors labeled on figures, these regions approximately cover (1) dorsal precentral, paracentral, and posterior cingulate; (2) insula; (3) isthmus cingulate; (4) lateral precentral and postcentral; (5) temporal pole; (6) inferior frontal; (7) medial temporal; (8) superior temporal; (9) supra marginal; (10) dorsal superior frontal; (11) caudal middle frontal; (12) precuneus; (13) superior parietal; (14) medial occipital; (15) medial prefrontal; (16) dorsal prefrontal; (17) middle and inferior temporal; and (18) lateral occipital.

To further explore the hierarchical relationship between these 18 regions, the dendrogram was leveraged for its advantage in illustrating the hierarchical organization as employed in previous studies (32, 42, 45). Specifically, the surface area of each region of each scan was first normalized based on its corresponding total surface area. Next, the correlations of the normalized surface area between any two regions across all scans were estimated. Finally, a dendrogram based on the correlations was formed to demonstrate the hierarchical relationship between regions (Fig. 3*B*). We found that the 18 regions can be classified into three hierarchical groups: (1) dorsal precentral, paracentral, and posterior cingulate (region 1); insula (region 2); isthmus cingulate (region 3); and lateral precentral and postcentral (region 4), (2) temporal pole (region 5); inferior frontal (region 6); medial temporal (region 7); superior temporal (region 8); supra marginal (region 9); dorsal superior frontal (region 10); caudal middle frontal (region 11); precuneus (region 12); superior parietal (region 13); medial occipital (region 14); and medial prefrontal (region 15), and (3) dorsal prefrontal (region 16); middle and inferior temporal (region 17); and lateral occipital (region 18). Note that dorsal precentral, paracentral, and posterior cingulate (region 1); insula (region 2); and isthmus cingulate (region 3) are more similar with each other than with lateral precentral and postcentral (region 4) in group 1. Dorsal prefrontal (region 16) and middle and inferior temporal (region 17) are more similar with each other than with lateral occipital (region 18) in group 3.

Additionally, to investigate the change of the organization among developmental regions along the time, we divided the

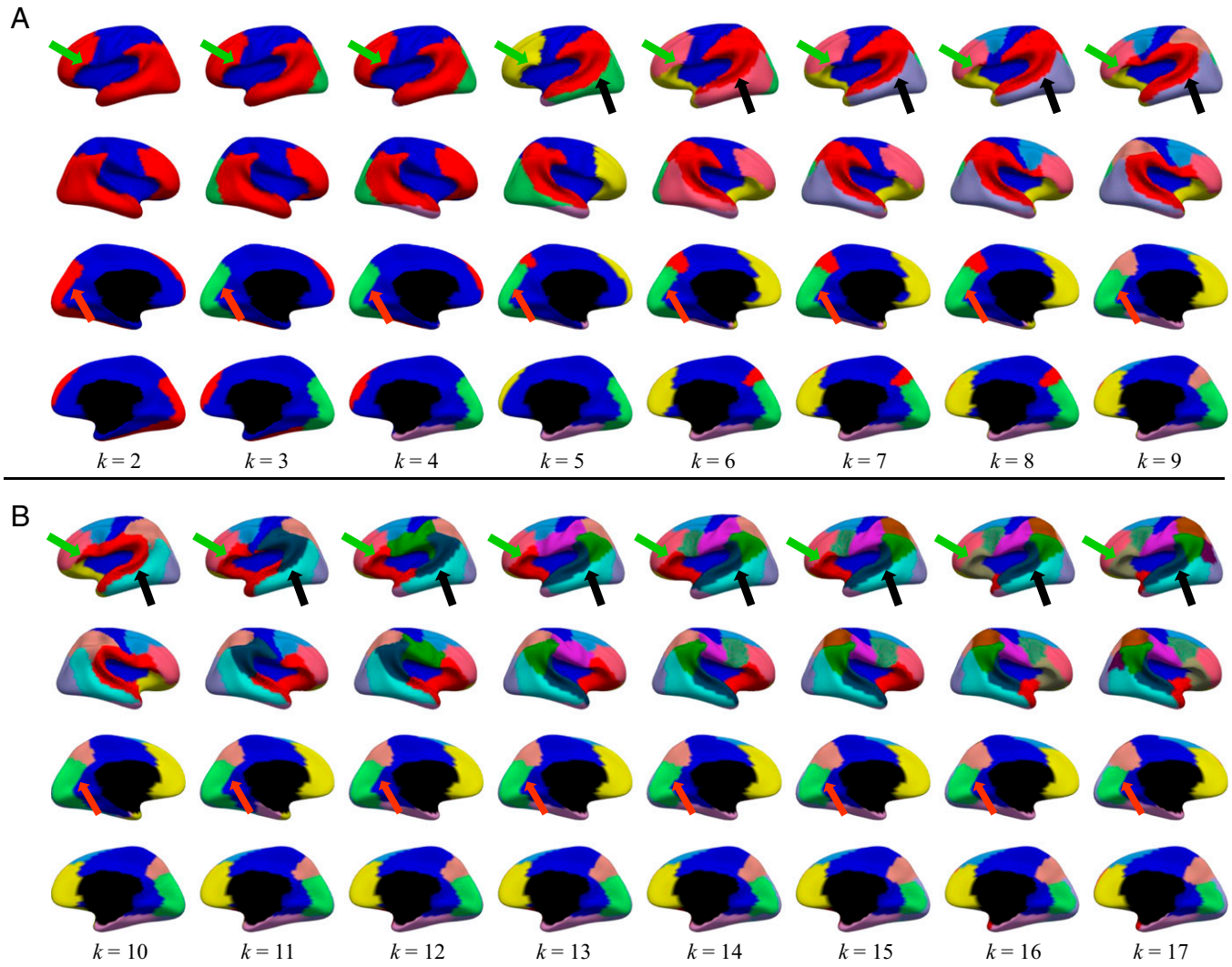


**Fig. 1.** Developmental regionalization maps of cortical surface area on the left and right hemispheres from 29 post-menstrual weeks to 2 y of age, with the region numbers *k* increasing from 2 to 17. Arrows point to some well-preserved regional boundaries when the region number increases.

two datasets (dHCP and BCP) into three age groups: age group 1 (dHCP from 29 to 45 post-menstrual weeks), age group 2 (BCP from 0.3 to 12 postnatal months), and age group 3 (BCP from 12 to 24 postnatal months). For each age group, we delineated the organization among the developmental regions based on the discovered 18 regions from the combined dHCP and BCP datasets, with results shown in Fig. 3 *C*–*E*. For age group 1, the developmental organization of surface area exhibits two major distinct components, which contain (1) the medial cortices, occipital cortex, and insula cortex and (2) the temporal, lateral frontal, and parietal cortices. For age group 2, the organization among developmental regions demonstrates

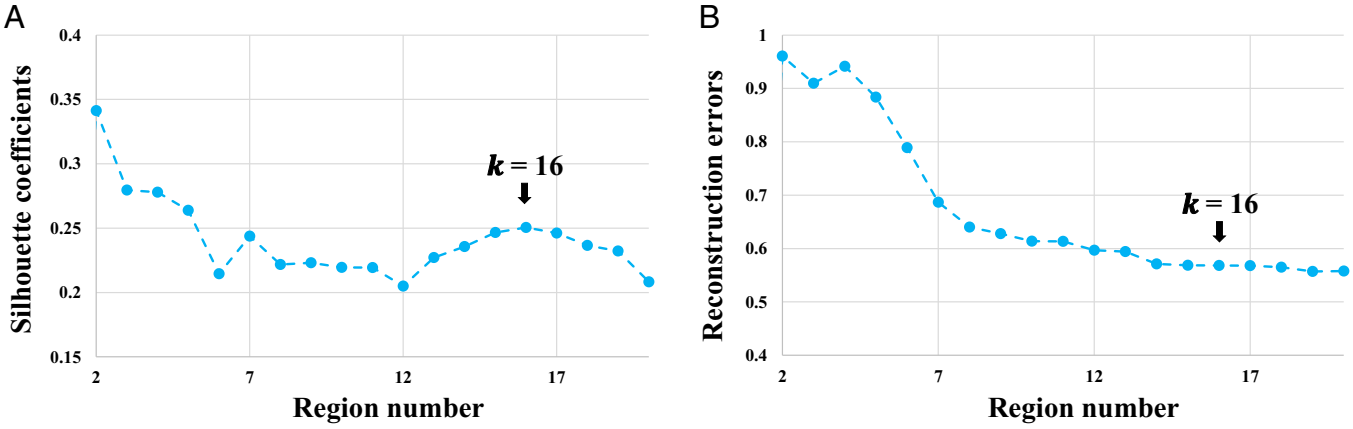


**Fig. 2.** Criteria for determining the appropriate region number. (*A*) Silhouette coefficients. (*B*) Reconstruction errors. The black arrows indicate the appropriate region number with a high silhouette coefficient and a relatively low reconstruction error.

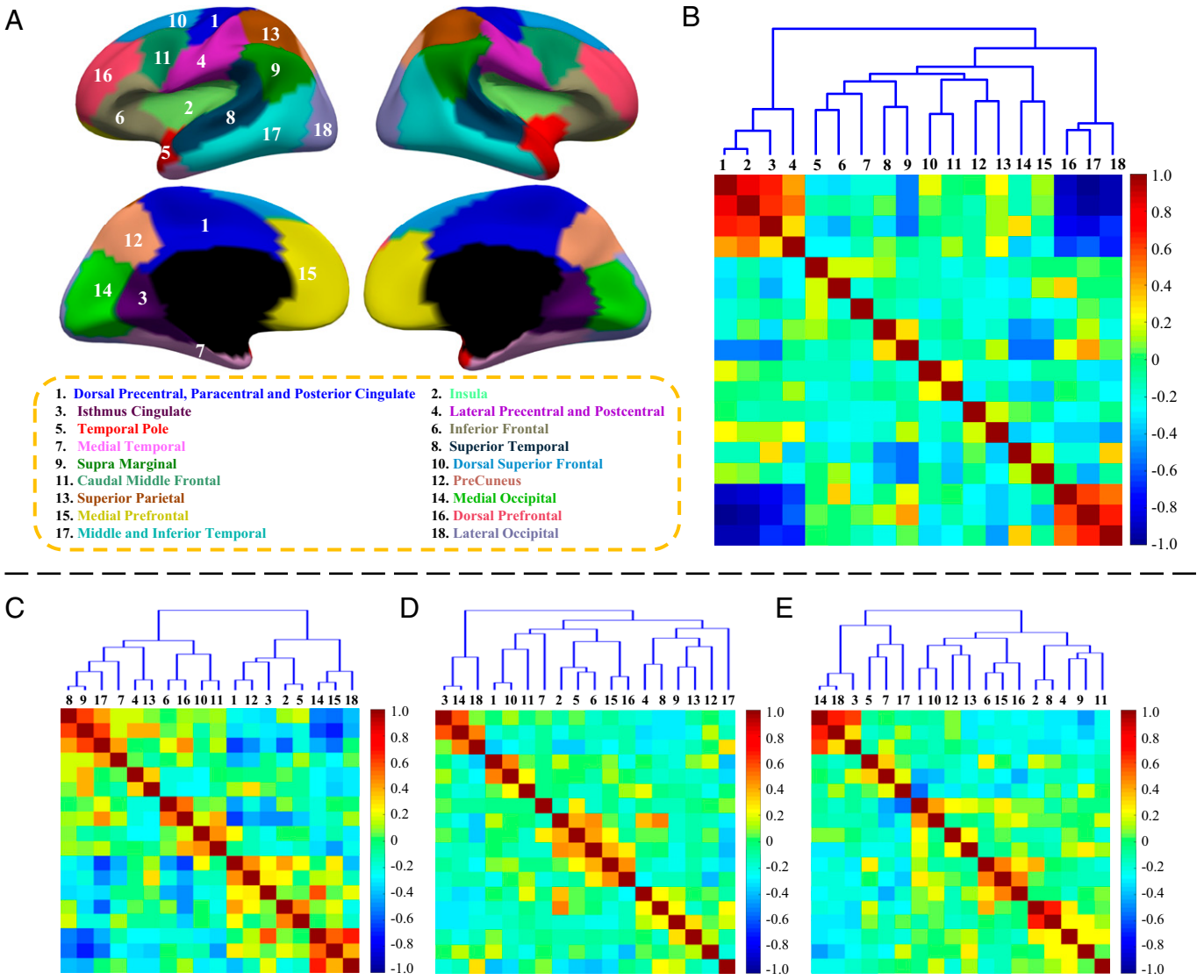


**Fig. 3.** Organization among developmental regions from different ages. (*A*) Discovered cortical developmental regionalization map with 18 regions based on the developmental patterns of surface area from 29 post-menstrual weeks to 24 postnatal months of age. (*B*) The dendrogram of the 18 regions in our discovered developmental regionalization map. (*C*) The dendrogram among the 18 discovered regions from dHCP with age between 29 and 45 post-menstrual weeks. (*D*) The dendrogram among the 18 discovered regions from BCP with age between 0.3 and 12 postnatal months of age. (*E*) The dendrogram among the 18 discovered regions from BCP with age between 12 and 24 postnatal months of age. The color scale encodes the correlations between regions.

three different parts: (1) the anterior frontal and insular cortices, (2) the posterior parietal and temporal cortices, and (3) the posterior occipital cortex. For age group 3, the cerebral cortex can be roughly divided into three parts: (1) the temporal and occipital cortices, (2) the prefrontal-parietal cortices, and (3) the cortices around the sylvian fissure (e.g., insula, superior temporal, lateral precentral and postcentral, supramarginal, and caudal middle frontal cortices).

**Developmental Pattern of Each Discovered Region.** Based on the discovered 18 regions, we applied the GAMM method to model the developmental pattern of surface area in each region. The overall developmental trajectories on both left and right hemispheres in the same region are largely similar (Fig. 4 and *SI Appendix*, Fig. S2). All regions exhibit dramatic expansion in surface area, with each region showing a distinct developmental trajectory. Moreover, the growth rate of surface area in the earlier stage is much higher than that in the later stage. Significant gender differences after controlling of the total brain surface area appear only in a few regions (*SI Appendix*, Table S1) of both hemispheres, with males having larger surface area than females. Specifically, for the left hemisphere, in the caudal middle frontal (region 11), medial prefrontal (region 15), and inferior temporal (region 17), significant gender differences present between 3.8 and 6.5 postnatal months, while a little later in the isthmus cingulate (region 3), with significant gender difference starting at 20.9 postnatal months. As for the right hemisphere, significant gender differences exist in the posterior cingulate (region 1), isthmus cingulate (region 3), and the dorsal superior frontal (region 10), with the starting ages at 6.5, 9.3, and 5.7 postnatal months, respectively.

To further compare the developmental paces of surface area in the discovered 18 regions, each fitted curve was normalized by its value at the term-born post-menstrual age of 40 wk (Fig. 5 *A* and *B*). Though the surface area of each region exhibits dynamic increase with age during perinatal and early postnatal stages, the developmental paces vary dramatically across regions. By performing the K-means clustering based on the differences of normalized surface areas between each region and the whole brain at 24 mo (Fig. 5), regional developmental trajectories can

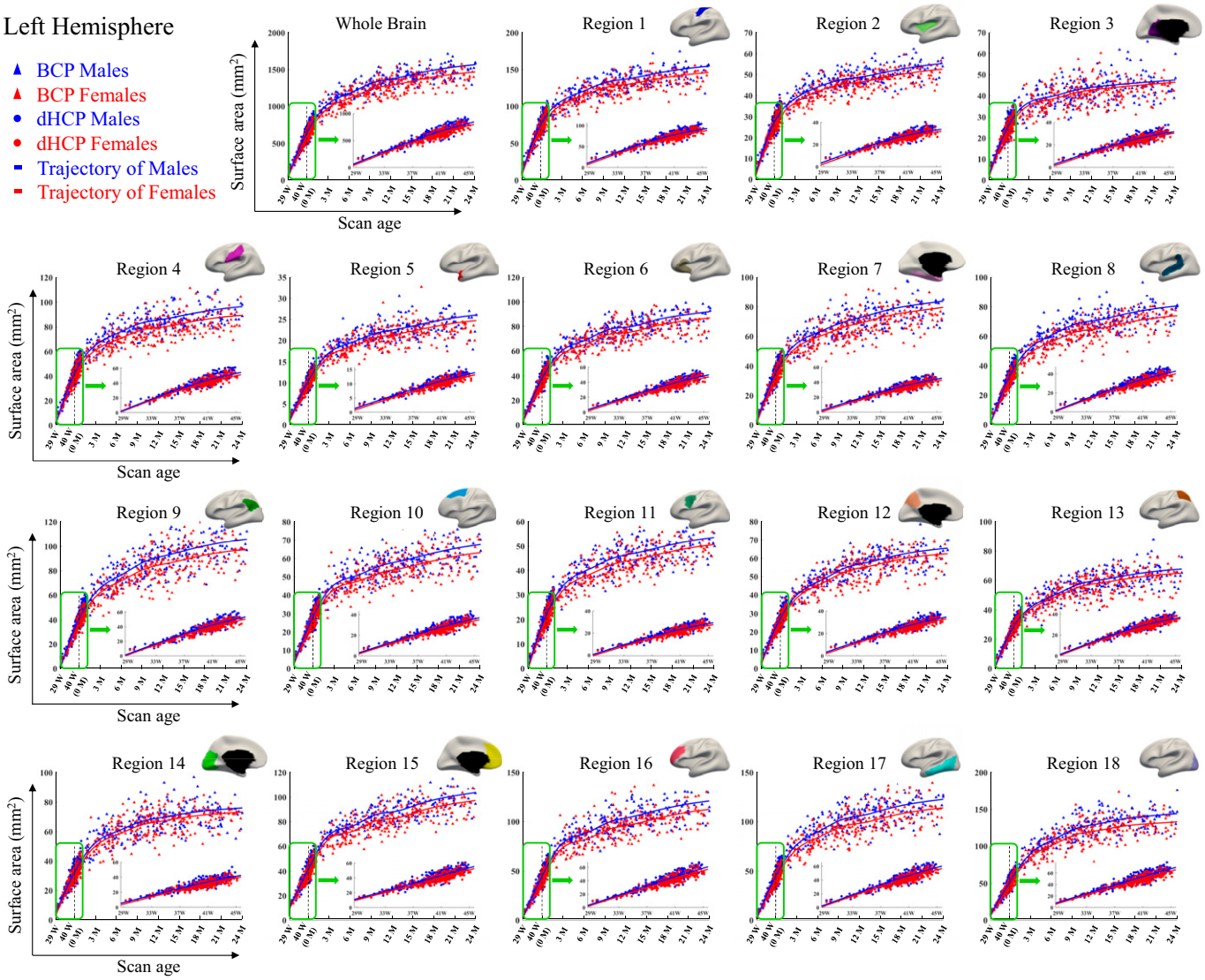


**Fig. 4.** Developmental trajectories of surface areas of the 18 regions in our discovered regionalization map of the left hemisphere. The x-axis denotes the scan age and the *y*-axis denotes the total/regional surface area. The W and M represent the (post-menstrual) weeks and (postnatal) months, respectively. Blue and red colors represent males and females, respectively. The filled triangles and dots represent data from the BCP and the dHCP, respectively. The curves in each figure illustrate the fitted developmental trajectory of each region. Dashed lines in figures stand for 40 post-menstrual weeks. The data distribution of the dHCP is framed by the green rectangle and enlarged in the right corner of each figure.

be divided into three categories: (1) regions exhibiting much slower development than the whole cerebral cortex, including dorsal precentral, paracentral, and posterior cingulate (region 1); insula (region 2); and isthmus cingulate (region 3), (2) regions having developmental paces similar with the whole cerebral cortex, including regions 4–15, and (3) regions exhibiting much faster development than the whole cerebral cortex, including regions 16–18. Using the stratified bootstrap (46) for longitudinal data with 1,000 times of resampling, we found that the normalized surface area of each region in category 1 is significantly smaller ($P < 1e{-}16$) than the normalized whole brain, while each region in category 3 is significantly larger ($P < 1e{-}16$) than the normalized whole brain. All the $P$ values are after Bonferroni correction for all 36 regions from both hemispheres. The three different developmental categories are exhibited with three different types of lines (Fig. 5 *A* and *B*). We also mapped the categories onto both hemispheres to show their spatial distribution on the cortical surface (Fig. 5*C*); the faster developing regions are colored in red, while the slower developing regions are colored in blue.

## Discussion

Several studies have been performed to investigate the development of surface area in early ages. However, they were based on small-sample data from very sparse imaging acquisition ages either in prenatal stages (42, 47–49) or postnatal stages (36, 39, 50, 51), thus cannot well characterize the dynamic and complex early brain development. In this paper, leveraging two complementary high-quality datasets, which cover both prenatal and early postnatal periods with high imaging resolution and dense time points in longitudinal designs and are carefully processed and aligned into the same space, we revealed the developmental regionalization of surface area from 29 post-menstrual weeks to 2 y of age. We found that the discovered regions are bilaterally relatively symmetric, despite that all the distinctive regions were naturally formed on two hemispheres independently and simultaneously without imposing any restrictions for hemispheric symmetry. Therefore, our results suggest that the development of surface area during this period is bilaterally symmetric. Moreover, the developmental patterns of cortical thickness during infancy (30),

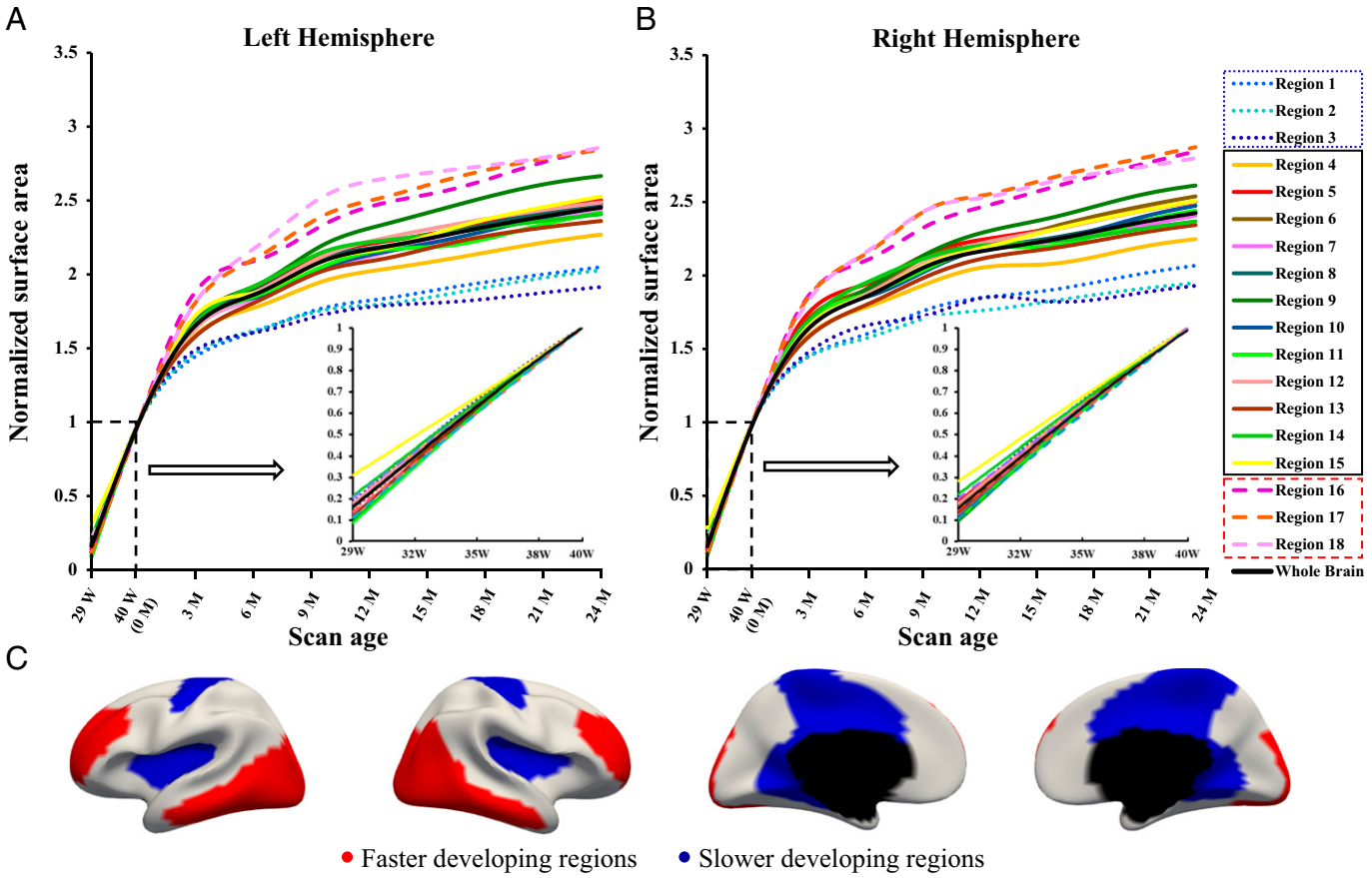


**Fig. 5.** Regional developmental trajectories of surface area and their developmental categories. (*A* and *B*) Normalized developmental trajectory of surface area in each discovered region. The x-axis denotes the scan age, and the *y*-axis denotes normalized surface area based on the values at 40 post-menstrual weeks. W and M represent weeks and months, respectively. The colored curves are the normalized developmental trajectories in different regions, while the black curves represent the normalized developmental trajectory of the whole cerebral cortex. Curves prior to 40 post-menstrual weeks are framed in black dashed lines and zoomed in to show the pace trend more clearly. (*C*) Three different developmental categories of surface area on both hemispheres. The red and blue regions represent regions developing faster and slower than the whole cerebral cortex, respectively.

genetic patterns of surface area in adults (32, 45, 52), and the cortical functional parcellation (53, 54) all demonstrate bilaterally relatively symmetric patterns. The underlying mechanism causing such hemispheric symmetries could be the regulation of genes or the communication between symmetric brain regions.

We found that the region number $k = 2$ leads to a distinct separation between central and pole regions as well as between lateral and medial regions. Specifically, the first cluster includes the lateral prefrontal, temporal, and occipital regions, which exhibit faster development of surface area, while the second cluster contains sensorimotor, insula, and medial cortices, which exhibit slower development of surface area. This is in line with the fact that the cortical folds in the second cluster are typically formed earlier during fetal brain development (55) and thus are more developed and established before birth and undergo less expansion during infancy, compared with the lateral prefrontal, temporal, and occipital regions. Indeed, during the first 2 postnatal years, the high-order association cortices (lateral prefrontal and temporal) exhibit high growth of cortical local gyrification, while the sensorimotor regions show low growth of cortical local gyrification (56). The mechanisms of this spatially heterogeneous cortical surface expansion are not sufficiently understood, but it likely relates to remarkable cellular, functional, and genetic nonuniformities varying during different developmental periods (57–59).

In our discovered cortical developmental regionalization map with 18 regions, several regions are consistent with previous genetic clustering maps of surface area in adults (32, 45). For example, region 7 (medial temporal), region 12 (precuneus), region 13 (superior parietal), region 16 (dorsal prefrontal), and region 17 (middle and inferior temporal) correspond well to their cluster 8, cluster 11, cluster 10, cluster 2, and cluster 7, respectively. Since the development of surface area undergoes complex and dynamic genetic and environmental influences across lifespan (50), such consistency may suggest that these regions are subject to strong genetic influences, leading to the formation of fixed genetic patterns at early ages. As for the inconsistent regions, they may be less genetically influenced while suffering from strong environmental influences during development. Of note, the genetic clustering maps of surface area were obtained in adults; for rigorous comparison and understanding genetic and environmental influences on surface area, longitudinal studies from infancy to adulthood should be performed in future.

We found large differences between our developmental regionalization and available infant cortical parcellations, indicating developmental boundaries are not confined by the infant structural and functional parcellation boundaries. As these infant structural and functional parcellations didn't consider and leverage rich cortical developmental information, such differences between conventional parcellations and our developmental regionalization are inevitable. In addition, we found that the developmental regionalization of surface area is very different from that of cortical thickness during infancy (30), suggesting that surface area and cortical thickness indeed have highly distinct developmental patterns and mechanisms.

We observed the organization patterns among developmental regions of surface area changes with age. In age group 1 (29–45 post-menstrual weeks), the development pattern of surface area approximately indicates a lateral-medial division. Previous studies on neonates (11, 60) also show the nonuniform cortical expansion after birth, with the lateral temporal, parietal, and frontal regions expanding much more than the insular and medial regions (11), in line with our finding. As in age group 2, adjacent cortices or within-lobe cortices exhibit more similar developmental patterns of surface area. A previous study indicates that large parts of the frontal and insula cortices exhibit different surface expansions compared with the parietal, temporal, and occipital lobes during the first postnatal year (39), largely supporting our results. In age group 3, the synchronized expansion patterns of surface area among regions might be related to the establishment of coordinated functions in this age period. For example, the cortical regions around the Sylvian fissure, which are mainly related to language function (e.g., Broca's area and Wernicke's area), demonstrate a synchronized development of surface area in our results, likely indicating the established connections of functionally specialized regions during the second year. Further structural and functional network analyses are needed to confirm our speculations.

Our results also suggest that the developmental patterns of surface area were variable across different time periods during early brain development. In the early age from 29 to 45 post-menstrual weeks, surface area expands almost linearly at a high speed. With the age increasing, surface area continues to expand dramatically, but the developmental pace gradually decreases. This is in accordance with previous studies demonstrating that surface area in the first year develops much faster than that in the second year (9, 39), based on their sparse data points at 1 mo, 1 y, and 2 y of age. Besides, the developmental rate of surface area in the first 2 y is much larger than that in older children and adolescents (10). Furthermore, before controlling the total brain surface area, we found gender differences of surface area (males > females) exist in all regions from the starting age in our study, i.e., 29 post-menstrual weeks. However, after controlling the total surface area, only a few regions have greater surface area in males than females. These results are in line with the previous studies, which indicate that gender differences exist in surface area and males have greater uncontrolled surface area in infants (33, 61) but the differences are greatly reduced after controlling for global covariates (9, 61).

**Limitations.** Although our discovered developmental regionalization of surface area reveals neurobiologically meaningful regions with hierarchical and bilaterally symmetric patterns, certain limitations still exist in this study. First, we combined two complementary pediatric datasets acquired from different scanners with different imaging protocols, which may have influence on the results. Nevertheless, we processed these datasets carefully using dedicated tools and utilized the cortical surface area for discovering developmental regionalization, which is a relatively robust cortical feature and much less sensitive to imaging protocol than other cortical features, e.g., cortical thickness. From the overlapping age ranges of these datasets, we can also see their developmental trajectories are very similar. Second, our regionalization map was obtained only based on a single cortical feature, i.e., surface area. Since each cortical feature has its unique neurobiological mechanisms, a single cortical feature absolutely cannot comprehensively characterize the cortical developmental regionalization. In the future, we will take multiple distinct cortical features into account to jointly characterize the cortical developmental regionalization. To this end, we may need to do harmonization of cortical features from multisite datasets as described in (62).

**Conclusion.** In this study, we leveraged two large complementary datasets, which seamlessly cover the most intensively and dynamically developmental periods of the human brain, to unprecedently discover the developmental patterns and regionalization of cortical surface area from 29 post-menstrual weeks to 2 y of age. We revealed the bilaterally symmetric and hierarchical organization of the developmental regionalization of cortical surface. Based on the discovered regions, we explicitly fitted their distinct developmental trajectories, revealed the gender differences starting from early postnatal stages, and illustrated the fast and slow developing regions of surface area located in the high-order associate cortices and central regions, respectively. These discoveries provide fundamental insights for understanding both normal and abnormal early brain development. In future, we will further extend the age range of our study, e.g., including earlier prenatal stages.

## Materials and Methods

**Informed Consent and Institutional Review Board.** The Institutional Review Boards at The University of North Carolina at Chapel Hill approved this study. Informed consent for experiments was obtained prior to imaging.

**Participants.** Two complementary high-quality and public imaging datasets on early brain development, i.e., the dHCP and the BCP, were included in this study (*SI Appendix*, Fig. S1 and *SI Appendix*, Table S3). The dHCP dataset used in this study contains 549 MRI scans acquired from 500 (279 males/221 females) healthy neonates with scan age from 29 to 45 post-menstrual weeks (40). MR images were acquired on a Philips 3T scanner (St. Thomas Hospital, London, UK) with a 32-channel neonate-dedicated head coil (63). The BCP dataset used in this study contains 488 longitudinal MRI scans from 235 (108 males/127 females) healthy, term-born infants with the scan age between 0.3 mo and 24 mo. Images were collected on 3T Siemens Prisma MRI scanners using a Siemens 32-channel head coil at The University of North Carolina (UNC) at Chapel Hill and University of Minnesota (41). See full methods in *SI Appendix, SI Materials and Methods*.

**Revealing the Developmental Regionalization of Surface Area.** To reveal the developmental regionalization of the dynamic cortical surface area expansion during pregnancy and infancy, we employed a data-driven method, i.e., NMF method, to partition the cortical surface into a set of distinct regions based on the developmental patterns of surface area via clustering cortical vertices with similar developmental patterns into the same region. Specifically, a nonnegative data matrix $\boldsymbol{V}$ was first constructed by organizing each data sample into one column. Then, the NMF was employed to decompose $\boldsymbol{V}$ into the base/component matrix $\boldsymbol{W}$ and coefficient matrix $\boldsymbol{H}$, i.e., $\boldsymbol{V} \approx \boldsymbol{W} \times \boldsymbol{H}$. The nonnegative factors in each column of $\boldsymbol{W}$ intrinsically corresponded to a set of cortical vertices with similar developmental pattern and thus can be considered as a meaningful subregion in developmental regionalization (30, 44). To evaluate the quality of the discovered regionalization results with different region numbers and subsequently discover the appropriate region number, we jointly utilized the silhouette coefficient (64) and reconstruction error. The appropriate region number was obtained with a high silhouette coefficient and a low reconstruction error. See full method in *SI Appendix*.

**Statistical Analysis.** First, considering the nonlinear and dynamic nature of the development of cortical surface area during infancy, we adopted the nonparametric GAMM to explicitly model the developmental trajectory of each region. Then, to test the significant gender differences of surface areas in each region, we constructed 95% Bonferroni simultaneous confidence intervals with correction for $k$ regions and the whole brain following the methods in (65, 66). Age ranges with significant gender difference were determined when the confidence intervals did not include zero. The above steps were carried out with the R package itsadug. Next, for each of the $k$ regions and the whole brain, we calculated the normalized surface area based on their corresponding values at 40 post-menstrual weeks. Based on the differences of normalized surface area

between each region and the whole brain at 24 mo of age, the K-means clustering algorithm was adopted to classify the $k$ regions of both left and right hemispheres into three clusters, respectively. Finally, by leveraging stratified bootstrap for data (46) with 1,000 times of resampling, we test the significant difference of normalized surface area between each region in the three clusters and the whole brain at 24 mo. See full method in *SI Appendix, SI Materials and Methods*.

**Data Availability.** All data used to draw the conclusions in our work were detailedly described in the article and/or *SI Appendix*. The dHCP dataset is publicly available at the Developing Human Connectome Project repository: http://www.developingconnectome.org/ (67). The BCP dataset is publicly available in NIMH Data Archive: https://nda.nih.gov/edit_collection.html?id=2848 (68).

**ACKNOWLEDGMENTS.** This work was supported in part by NIH grants: MH116225, MH117943, and MH123202. This work also utilizes approaches developed by an NIH grant (1U01MH110274) and the efforts of the UNC/UMN Baby Connectome Project Consortium.

Author affiliations: [a]School of Automation, Northwestern Polytechnical University, Xi'an 710071, China; and [b]Department of Radiology and Biomedical Research Imaging Center, The University of North Carolina at Chapel Hill, Chapel Hill, NC 27599

1. T. T. Brown, T. L. Jernigan, Brain development during the preschool years. *Neuropsychol. Rev.* **22**, 313–333 (2012).
2. J. Stiles, T. L. Jernigan, The basics of brain development. *Neuropsychol. Rev.* **20**, 327–348 (2010).
3. A. L. Tierney, C. A. Nelson III, Brain development and the role of experience in the early years. *Zero Three* **30**, 9–13 (2009).
4. R. Cafiero, J. Brauer, A. Anwander, A. D. Friederici, The concurrence of cortical surface area expansion and white matter myelination in human brain development. *Cereb. Cortex* **29**, 827–837 (2019).
5. R. Haartsen, E. J. Jones, M. H. Johnson, Human brain development over the early years. *Curr. Opin. Behav. Sci.* **10**, 149–154 (2016).
6. H. Huang *et al.*, Development of human brain structural networks through infancy and childhood. *Cereb. Cortex* **25**, 1389–1404 (2015).
7. G. Li *et al.*, Computational neuroanatomy of baby brains: A review. *Neuroimage* **185**, 906–925 (2019).
8. R. A. I. Bethlehem *et al.*; 3R-BRAIN; AIBL; Alzheimer's Disease Neuroimaging Initiative; Alzheimer's Disease Repository Without Borders Investigators; CALM Team; Cam-CAN; CCNP; COBRE; cVEDA; ENIGMA Developmental Brain Age Working Group; Developing Human Connectome Project; FinnBrain; Harvard Aging Brain Study; IMAGEN; KNE96; Mayo Clinic Study of Aging; NSPN; POND; PREVENT-AD Research Group; VETSA, Brain charts for the human lifespan. *Nature* **604**, 525–533 (2022).
9. A. E. Lyall *et al.*, Dynamic development of regional cortical thickness and surface area in early childhood. *Cereb. Cortex* **25**, 2204–2212 (2015).
10. L. M. Wierenga, M. Langen, B. Oranje, S. Durston, Unique developmental trajectories of cortical thickness and surface area. *Neuroimage* **87**, 120–126 (2014).
11. K. E. Garcia *et al.*, Dynamic patterns of cortical expansion during folding of the preterm human brain. *Proc. Natl. Acad. Sci. U.S.A.* **115**, 3156–3161 (2018).
12. F. J. Román *et al.*, Cortical surface area variations within the dorsolateral prefrontal cortex are better predictors of future cognitive performance than fluid ability and working memory. *Psicothema* **31**, 229–238 (2019).
13. J. Piven, J. T. Elison, M. J. Zylka, Toward a conceptual framework for early brain and behavior development in autism. *Mol. Psychiatry* **23**, 165 (2018).
14. L. Chen *et al.*, A 4D infant brain volumetric atlas based on the UNC/UMN baby connectome project (BCP) cohort. *Neuroimage* **253**, 119097 (2022).
15. L. Feng *et al.*, Age-specific gray and white matter DTI atlas for human brain at 33, 36 and 39 postmenstrual weeks. *Neuroimage* **185**, 685–698 (2019).
16. I. S. Gousias *et al.*, Automatic segmentation of brain MRIs of 2-year-olds into 83 regions of interest. *Neuroimage* **40**, 672–684 (2008).
17. K. Oishi, L. Chang, H. Huang, Baby brain atlases. *Neuroimage* **185**, 865–880 (2019).
18. G. Li *et al.*, Construction of 4D high-definition cortical surface atlases of infants: Methods and applications. *Med. Image Anal.* **25**, 22–36 (2015).
19. Z. Wu *et al.*, Construction of 4D infant cortical surface atlases with sharp folding patterns via spherical patch-based group-wise sparse representation. *Hum. Brain Mapp.* **40**, 3860–3880 (2019).
20. J. Bozek *et al.*, Construction of a neonatal cortical surface atlas using multimodal surface matching in the developing human connectome project. *Neuroimage* **179**, 11–29 (2018).
21. Z. Wu *et al.*, "Construction of spatiotemporal neonatal cortical surface atlases using a large-scale dataset" in *2018 IEEE 15th International Symposium on Biomedical Imaging (ISBI 2018)* (IEEE, 2018), pp. 1056–1059.
22. F. Shi, A. P. Salzwedel, W. Lin, J. H. Gilmore, W. Gao, Functional brain parcellations of the infant brain and the associated developmental trends. *Cereb. Cortex* **28**, 1358–1368 (2018).
23. F. Shi *et al.*, Infant brain atlases from neonates to 1- and 2-year-olds. *PLoS One* **6**, e18746 (2011).
24. L. Zöllei, J. E. Iglesias, Y. Ou, P. E. Grant, B. Fischl, Infant FreeSurfer: An automated segmentation and surface extraction pipeline for T1-weighted neuroimaging data of infants 0-2 years. *Neuroimage* **218**, 116946 (2020).
25. I. S. Gousias *et al.*, Magnetic resonance imaging of the newborn brain: Manual segmentation of labelled atlases in term-born and preterm infants. *Neuroimage* **62**, 1499–1509 (2012).
26. K. Oishi *et al.*, Multi-contrast human neonatal brain atlas: Application to normal neonate development analysis. *Neuroimage* **56**, 8–20 (2011).
27. B. Alexander *et al.*, A new neonatal cortical and subcortical brain atlas: The Melbourne Children's Regional Infant Brain (M-CRIB) atlas. *Neuroimage* **147**, 841–851 (2017).
28. C. L. Adamson *et al.*, Parcellation of the neonatal cortex using surface-based Melbourne Children's Regional Infant Brain atlases (M-CRIB-S). *Sci. Rep.* **10**, 4359 (2020).
29. J. Zhu *et al.*, Integrated structural and functional atlases of Asian children from infancy to childhood. *Neuroimage* **245**, 118716 (2021).
30. F. Wang *et al.*, Developmental topography of cortical thickness during infancy. *Proc. Natl. Acad. Sci. U.S.A.* **116**, 15855–15860 (2019).
31. A. B. Storsve *et al.*, Differential longitudinal changes in cortical thickness, surface area and volume across the adult life span: Regions of accelerating and decelerating change. *J. Neurosci.* **34**, 8488–8498 (2014).
32. C.-H. Chen *et al.*, Genetic topography of brain morphology. *Proc. Natl. Acad. Sci. U.S.A.* **110**, 17089–17094 (2013).
33. J. H. Gilmore, R. C. Knickmeyer, W. Gao, Imaging structural and functional brain development in early childhood. *Nat. Rev. Neurosci.* **19**, 123–137 (2018).
34. H. C. Hazlett *et al.*, Early brain overgrowth in autism associated with an increase in cortical surface area before age 2 years. *Arch. Gen. Psychiatry* **68**, 467–476 (2011).
35. R. C. Knickmeyer *et al.*, A structural MRI study of human brain development from birth to 2 years. *J. Neurosci.* **28**, 12176–12182 (2008).
36. G. Li *et al.*, Cortical thickness and surface area in neonates at high risk for schizophrenia. *Brain Struct. Funct.* **221**, 447–461 (2016).
37. H. G. Schnack *et al.*, Changes in thickness and surface area of the human cortex and their relationship with intelligence. *Cereb. Cortex* **25**, 1608–1617 (2015).
38. K. B. Walhovd *et al.*, Neurodevelopmental origins of lifespan changes in brain and cognition. *Proc. Natl. Acad. Sci. U.S.A.* **113**, 9357–9362 (2016).
39. G. Li *et al.*, Mapping region-specific longitudinal cortical surface expansion from birth to 2 years of age. *Cereb. Cortex* **23**, 2724–2733 (2013).
40. A. Makropoulos *et al.*, The developing human connectome project: A minimal processing pipeline for neonatal cortical surface reconstruction. *Neuroimage* **173**, 88–112 (2018).
41. B. R. Howell *et al.*, The UNC/UMN baby connectome project (BCP): An overview of the study design and protocol development. *Neuroimage* **185**, 891–905 (2019).
42. J. Xia *et al.*, Fetal cortical surface atlas parcellation based on growth patterns. *Hum. Brain Mapp.* **40**, 3881–3899 (2019).
43. X. Lin, D. Zhang, Inference in generalized additive mixed modelsby using smoothing splines. *J. R. Stat. Soc. B* **61**, 381–400 (1999).
44. A. Sotiras *et al.*, Patterns of coordinated cortical remodeling during adolescence and their associations with functional specialization and evolutionary expansion. *Proc. Natl. Acad. Sci. U.S.A.* **114**, 3527–3532 (2017).
45. C.-H. Chen *et al.*, Hierarchical genetic organization of human cortical surface area. *Science* **335**, 1634–1636 (2012).
46. M. Sherman, S. I. Cessie, A comparison between bootstrap methods and generalized estimating equations for correlated outcomes in generalized linear models. *Commun. Stat. Simul. Comput.* **26**, 901–925 (1997).
47. Z. Zhang *et al.*, Development of the fetal cerebral cortex in the second trimester: Assessment with 7T postmortem MR imaging. *AJNR Am. J. Neuroradiol.* **34**, 1462–1467 (2013).
48. J. Dubois, G. Dehaene-Lambertz, "Fetal and postnatal development of the cortex: MRI and genetics" in *Brain Mapping: An Encyclopedic Reference*, A. W. Toga, Ed. (Elsevier Inc., 2015) pp.11–19.
49. L. Vasung *et al.*, Quantitative and qualitative analysis of transient fetal compartments during prenatal human brain development. *Front. Neuroanat.* **10**, 11 (2016).
50. S. C. Jha *et al.*, Genetic influences on neonatal cortical thickness and surface area. *Hum. Brain Mapp.* **39**, 4998–5013 (2018).
51. J. Remer *et al.*, Quantifying cortical development in typically developing toddlers and young children, 1-6 years of age. *Neuroimage* **153**, 246–261 (2017).
52. C.-H. Chen *et al.*, Genetic influences on cortical regionalization in the human brain. *Neuron* **72**, 537–544 (2011).
53. X. Shen, F. Tokoglu, X. Papademetris, R. T. Constable, Groupwise whole-brain parcellation from resting-state fMRI data for network node identification. *Neuroimage* **82**, 403–415 (2013).
54. B. T. Yeo *et al.*, The organization of the human cerebral cortex estimated by intrinsic functional connectivity. *J. Neurophysiol.* **106**, 1125–1165 (2011).
55. J. G. Chi, E. C. Dooling, F. H. Gilles, Gyral development of the human brain. *Ann. Neurol.* **1**, 86–93 (1977).
56. G. Li *et al.*, Mapping longitudinal development of local cortical gyrification in infants from birth to 2 years of age. *J. Neurosci.* **34**, 4228–4238 (2014).
57. P. Rakic, "Radial unit hypothesis of neocortical expansion" in *Novartis Foundation Symposium* (John Wiley, Chichester and New York, 1999), pp. 30–52 (2000).
58. C. E. Collins, D. C. Airey, N. A. Young, D. B. Leitch, J. H. Kaas, Neuron densities vary across and within cortical areas in primates. *Proc. Natl. Acad. Sci. U.S.A.* **107**, 15927–15932 (2010).
59. V. Fernández, C. Llinares-Benadero, V. Borrell, Cerebral cortex expansion and folding: What have we learned? *EMBO J.* **35**, 1021–1044 (2016).
60. J. Hill *et al.*, Similar patterns of cortical expansion during human development and evolution. *Proc. Natl. Acad. Sci. U.S.A.* **107**, 13135–13140 (2010).
61. T. J. Herron, X. Kang, D. L. Woods, Sex differences in cortical and subcortical human brain anatomy. *F1000 Res.* **4**, 88 (2015).
62. F. Zhao *et al.*, "Harmonization of infant cortical thickness using surface-to-surface cycle-consistent adversarial networks" in *International Conference on Medical Image Computing and Computer-Assisted Intervention* (Springer, 2019), pp. 475–483.
63. E. J. Hughes *et al.*, A dedicated neonatal brain imaging system. *Magn. Reson. Med.* **78**, 794–804 (2017).
64. P. J. Rousseeuw, Silhouettes: A graphical aid to the interpretation and validation of cluster analysis. *J. Comput. Appl. Math.* **20**, 53–65 (1987).
65. D. Ruppert, M. P. Wand, R. J. Carroll, *Semiparametric Regression* (Cambridge University Press, 2003).
66. G. Simpson, Simultaneous intervals for derivatives of smooths revisited. https://www.r-bloggers.com/2017/03/simultaneous-intervals-for-derivatives-of-smooths-revisited-2/. Deposited 21 March 2017.
67. Developing Human Connectome Project. http://www.developingconnectome.org/project. Accessed 23 September 2019.
68. J. Elison, W. Lin, UNC/UMN Baby Connectome Project. NIMH Data Archive. https://nda.nih.gov/edit_collection.html?id=2848. Deposited 15 July 2019.